JOURNAL OF OPTOELECTRONICS AND ADVANCED MATERIALS Vol. 9, No. 5, May 2007, p. 1382 - 1394

Invited Paper

Defects induced by ionizing radiations in A^{II}-B^{VI} pollycrystalline thin films used as solar cell materials

S. ANTOHE*, L. ION, V. A. ANTOHE, M. GHENESCU, H. ALEXANDRU
University of Bucharest, Faculty of Physics, P.O.Box: MG-11, Bucharest-Magurele, 077125 Romania

Thin films of $A^{II}B^{VI}$ compounds are potential candidates for the manufacturing of electronic and optoelectronic devices, especially solar cells. In this paper the effects of irradiation with high-energy electrons and protons on structural, electrical and optical properties of CdS and CdSe thin films have been investigated. The films, 1-3 μm thick, were prepared by thermal-vacuum evaporation on glass substrate at a temperature of 220 °C. The samples were irradiated with 6-7 MeV electrons, up to a fluency of 10^{17} e/cm^2 and with 3 MeV protons, up to a fluency of 10^{13} protons/cm^2, respectively. XRD investigation has revealed that the films contain wurtzite-type CdS and CdSe, (001) preferentially oriented in the growth direction. The defects induced by ionizing radiations have been studied by using various techniques: the space-charge-limited-current (SCLC) measurements, the thermally stimulated current spectroscopy (TSC), and the absorption and photoluminscence (PL) spectra measurements. It was found that the electrical conduction of the samples, both before and after irradiation, is controlled by different types of defect distributions, placed in the band gap of the investigated semiconducting layers. Parameters of identified defect levels were determined. A detailed discussion about the possible origin of these defects has been done, suggesting that the mainly defects induced by high-energy electron and proton irradiations are related with chalcogens (S or Se) vacancies. The origin of the other identified defects, with smaller ionization energies, remains unknown at this time.

(Received November 14, 2006; accepted April 12, 2007)

Keywords: Polycrystalline layers, CdS, CdSe, Electrons and protons irradiation

1. Introduction

$A^{II}B^{VI}$ compounds are good candidates for practical applications like solar cells, optical detectors and optoelectronic devices. Among them, cadmium sellenide (CdSe) and cadmium sulfide (CdS) are recommended by a suitable band gap and optical properties as very promising materials for optoelectronic devices, especially for solar energy conversion applications. It is well known that the performance of the devices based on thin films strongly depends on structural and electronic properties of the films obtained under various experimental conditions. Therefore, the task to identify and to learn how to control the defects having the most important influence on electrical and/or optical properties of the films is very important. Many reports have been published on the structural or electrical properties of vacuum deposited CdSe or CdS films [1-12]. However, little work was done on the influence of the ionizing radiations on their physical properties [10, 13-17]. Given that thin films of A^{II}-B^{VI} compounds, especially CdS, CdSe, CdTe, ZnSe, are suitable for producing solar cells used in space technology applications, where the flux of ionizing radiations is large, such a study is very important. Particularly, it is important to investigate the effect of proton irradiation, given the weight of 87% of protons in the cosmic rays. On the other hand, irradiation with electrons having energies in MeV range can also be used to investigate simple defects, like vacancies or interstitials, because in this case no massive structural damage is produced. An electron with energy of 1-10 MeV can only produce a small number of atomic displacements [18]. In this paper we present the results of a complex investigation of the changes induced by irradiation with electrons (6-7 MeV at fluencies up to 2×10^{17} e/cm^2) and protons (3 MeV, 3×10^{13} protons/cm^2) on the electrical properties of CdS and CdSe thin films, respectively. Different experimental techniques, well adapted for this type of investigations, were used (SCLC measurements and TSC spectroscopy, optical spectroscopy) and the results are discussed. A discussion of the possible origin of the main defects created by electron and proton irradiation concludes this work.

2. Experimental procedures

Thin films of CdS and CdSe, 1-3 μm thick, were prepared by thermal vacuum evaporation from a single source onto an optical glass substrate. The initial pressure in the evaporation cell was 2×10^{-5} Torr. The evaporator consisted of a quartz container heated to 750°C in the case of CdSe, and to 1100 ºC in the case of CdS. In both cases the substrates were maintained at 220 °C during the deposition. To improve the structural and chemical homogeneity of the films, they were subsequently thermally treated in vacuum at 300 °C, for 10 min.

Electrical investigations were performed on two types of structures, having respectively gold contacts in a

sandwich geometry Au/(CdSe or CdS)/Au and aluminum contacts in a planar geometry. The Au/(CdS or CdSe)/Au sandwich structures were prepared as follows: first a gold strip of 8 mm length, 2 mm width and 300 nm thickness was deposited on a glass plate substrate, then the CdS or CdSe film was grown on the gold electrode and, finally, a second gold strip was deposited on the semiconducting layer, having the same geometry as the first one but being placed in a perpendicular direction with respect to it. The effective area, formed by the overlap of the electrodes was 0.04 cm^2, of about one order of magnitude smaller than the area of CdS or CdSe film to prevent the edge effects. To improve the stability and ohmicity of the contacts, the structures were thermally treated in air at 250 °C, for 30 min. It is known [11,12,16] that the gold electrodes prepared in this way guarantee stable and relatively good ohmic contacts on CdS and CdSe thin films, respectively.

Planar structures were prepared by evaporating four Al contacts on top of CdS or CdSe films. The contacts, 1 mm × 1 mm in surface, 0.3 μm thick and separated by 1 mm, were placed in line.

The obtained structures were subjected to irradiation with electrons supplied by a betatron. The samples were irradiated at room temperature with 6-MeV and 7-MeV electrons to fluency up to 10^{17} electrons/cm^2, irradiation direction being perpendicular to the surface of the samples. The thermal effect during irradiation was negligible.

Proton irradiation was performed with protons supplied by an accelerator. Irradiation was carried out in an evacuated chamber, at ambient temperature, with 3 MeV protons to fluencies of 3×10^{13} protons/cm^2. During irradiation the distance between the output window of the accelerator and the sample was 20 cm and the thermal effect was negligible. The beam of incident protons supplied by the accelerator was directed perpendicularly to the surface of the samples.

The structure of the samples was investigated, before and after irradiation, with a θ-2θ X-ray diffractometer, using Cu-K□ (λ=1.54178 Å) line. Line profiles were recorded in a step-scanning regime with Δ(2θ)=0.05°. The temperature dependence of the electrical resistance and I-V characteristics were recorded by introducing the samples in a nitrogen cryostat or a He closed cycle cryostat and contacting the probes with soft Ag wire. During the measurements the pressure in cryostat was below 10^{-4} Torr. Electrical measurements were performed with a Keithley 2400 Source-Meter or a Philips X-Y recorder, in the temperature range allowed by the experimental setup.

Thermally stimulated current (TSC) analysis was performed after filling the traps by adequate illumination (540 nm light in the case of CdS, 700 nm light in the case of CdSe, for 15 min.) at 40 K. For a proper determination of ionization energies of the traps, a fractional heating technique was used.

3. Experimental results

A. Structure

As revealed by XRD spectra (Fig. 1), both CdS and CdSe films consist of a hexagonal compact (hcp) wurtzite phase, which is known to be the stable one for those compounds. The films are preferentially oriented with (001) crystalline direction perpendicular to their surface. The position of the peaks yields hcp lattice constants of 4.238Å (a_h) and 6.658Å (c_h) for CdS, respectively 4.296Å (a_h) and 7.030Å (c_h) for CdSe. While a_h is consistent with the reported bulk value, c_h is somewhat larger.

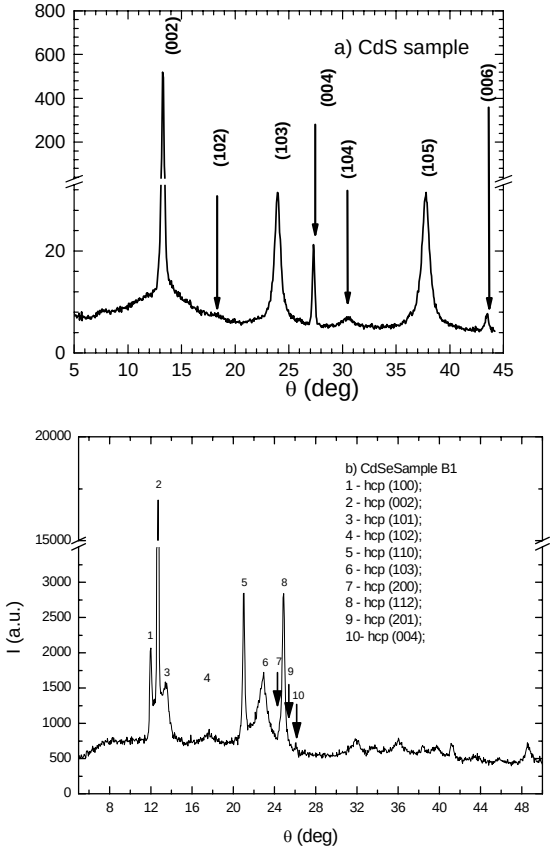

Fig. 1. X-ray diffraction pattern of CdS (a) and CdSe (b) thin films.

A simple inspection of the diffraction pattern shows that both broadened lines and sharp reflections are present. An explanation for this [19] has been given as due to faulting. In the case of crystals made up of close-packed layers of atoms, stacking faults (mistakes in the normal hexagonal or cubic packing order) may easily occur. The energy of producing such defects is very low. For reflections of the type (*hk*0), (00*l*) and (*hkl*) with *h*=*k*=3*n*, there is no change in structure factor on crossing the fault, therefore no broadening is observed. In contrast, for (*hkl*) reflections with *h*-*k*=3*n*±1, the structure factor changes significantly at each fault, which results in broadening the

line. The amount of broadening depends on the number of stacking faults.

The coherence lengths D_{eff}, calculated from (002) or (103) peaks, are indicated in Table 1. D_{eff} values were obtained using the well-known Scherrer formula:

$$D_{eff} = \frac{0.9\lambda}{\delta \cos\theta_0}, \quad (1)$$

where λ is the X-ray wavelength, θ_0 is the angle where the peak occurs and δ is its full width at half-maximum.

Table 1. Structural data, as determined from XRD spectra.

Sample	Lattice constants (Å)	D_{eff}(002) (Å)	D_{eff}(103) (Å)
CdS - A	a_h=4.238; c_h=6.658	907	132
CdSe – B1	a_h=4.296; c_h=7.030	1012	-

Within the limits of experimental resolution, no change in diffraction pattern aspect or in line broadening was observed following electron irradiation at fluencies up to 10^{17} electrons/cm^2 (Fig. 2). Therefore there are no major changes in the crystalline structure of the films, as a result of electron irradiation at energy and fluencies indicated above. It may be concluded that at most point-like defects (vacancies, interstitials or their association in some more complex defects) do occur in the structure of the films.

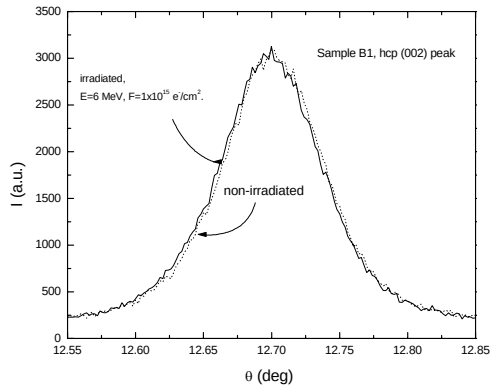

Fig. 2. X-ray diffraction pattern and hcp (002) peak for sample CdSe-B1, before and after irradiation.

B. Electrical properties – electron irradiated samples

B_1. Au/CdS/Au structures

$B_{1.1}$ The I - V characteristics before irradiation

The dark current - voltage characteristics of the Au/CdS/Au cells at 10 temperatures ranging from 197 to 374 K are shown in Fig. 3. The characteristics were completely symmetrical with respect to the polarity of applied voltage.

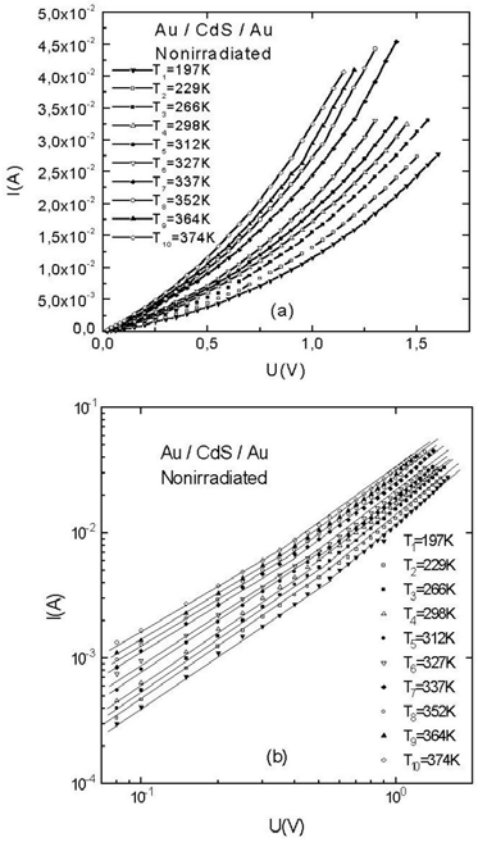

Fig. 3. The I-V characteristics of nonirradiated Au/CdS/Au cells for different temperatures: (a) in linear scale; (b) in logarithmic scale.

There are two distinct regions in these characteristics: at low voltages the slopes of the logI vs. logU plots are approximately equal to unity (1.08 - 1.18), while at higher voltages, above a well - defined transition voltage U_X, the slopes are approximately equal to two (exactly ranging from 1.7 to 2.14). These plots are typical of ohmic conduction for voltages below U_X and of space charge limited conductivity (SCLC) at voltages above U_X. This is a common feature for the most inorganic and organic layers [20], with low mobility and high resistivity. At low voltages the Ohm's law is followed, with a temperature dependence of the electrical conductivity well described by the expression:

$$\sigma(T) = \sigma_1 \exp\left(-\frac{E_{a1}}{k_B T}\right) + \sigma_2 \exp\left(-\frac{E_{a2}}{k_B T}\right), \quad (2)$$

as demonstrated by the plot in Fig. 4. The experimental results suggest that there are two competing conduction mechanisms: one of them, with larger activation energy and implying carriers in extended band states (conduction band mechanism) dominates in the high temperature

range, the other involving the hopping of the charge carriers over localized states in the band gap, induced by the structural and/or chemical disorder, dominates at low temperatures.

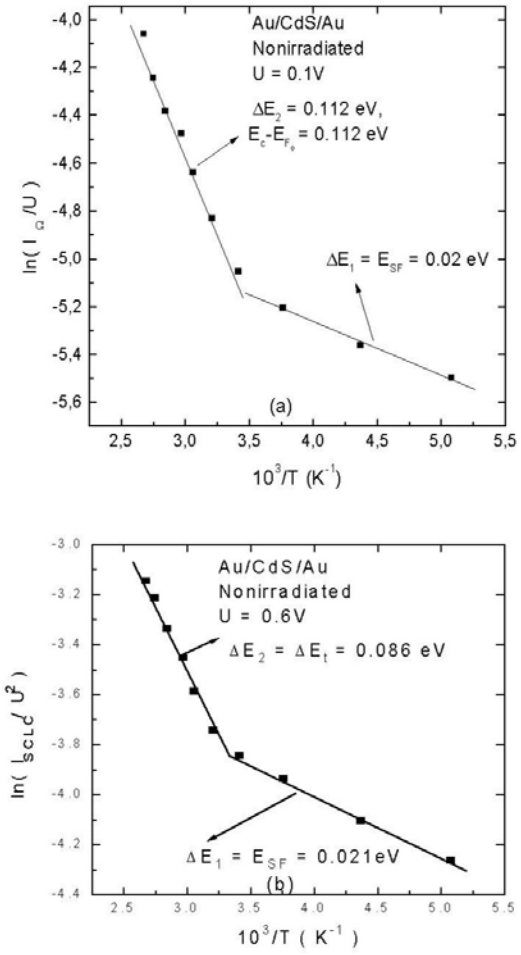

Fig. 4. (a) Dependence of ln (I_Ω / U) on the reciprocal temperature $10^3/T$ at U = 0.1 V; (b) Dependence of ln (I_{SCLC}/U^2) on reciprocal temperature $10^3/T$ at U = 0.6 V, for the Au/CdS/Au structures.

In the case of conduction band mechanism, the current density is given by:

$$j = \sigma(T)E = qn_0\mu\frac{U}{d} \tag{3}$$

where q is the electronic charge, $n_0 = N_c \exp\left[-E_{a1}/k_BT\right]$ is the equilibrium density of free electrons, N_c is the effective density of states in the conduction band (CB) of the grains, μ is the electron mobility, U is the applied voltage, $E_{a1}=E_c-E_{F0}$ is the separation of the equilibrium Fermi level from CB bottom edge, k_B is Boltzmann's constant and d is the film thickness.

From the plot of $ln(I_\Omega /U)$ versus $10^3/T$, for U = 0,1 V shown in Fig. 4a, the values E_{a1}=0.112 eV and $\mu_0 N_C$ = 2,17 $cm^{-1}V^{-1}s^{-1}$ were obtained by fit. $I_\Omega = j \times S$ is the current in the ohmic region, S being the effective area of the structures. At low temperatures, the activation energy of conductivity is E_{a2}=0.02 eV, a value which is typical for the hopping mechanism, being related with the activation energy of mobility.

For applied voltages greater than a transition voltage U_X , the slopes of *log I* versus *log U* characteristics in Fig. 3b are in the range of 1.8 to 2.1, indicating that the current is controlled by a space charge associated to a single dominant trap level. For this case, the current density may be expressed by the following equation [20]:

$$j_{SCLC} = \frac{9}{8}\varepsilon\mu_0\theta\frac{U^2}{d^3} \tag{4}$$

where in addition to the symbols defined above, ε represents the permittivity and θ is the ratio of the free to trapped carrier density, given by:

$$\theta = \frac{N_c}{N_t}\exp\left(-\frac{E_c - E_t}{k_BT}\right) \tag{5}$$

where N_t is the density of the trapping level located at the energy E_t below the CB edge. From eqs. (4,5), follows that:

$$j_{SCLC} = \frac{9}{8}\varepsilon\mu_0\frac{N_c}{N_t}\exp\left(-\frac{E_c - E_t}{k_BT}\right)\frac{U^2}{d^3} \tag{6}$$

and from the plot of $\ln\left(I_{SCLC}/U^2\right)$ versus $(1/T)$, the E_C-E_t and N_t values may be obtained. Figure 4(b) shows the dependence of $\ln\left(I_{SCLC}/U^2\right)$ versus $\left(10^3/T\right)$ for the voltage U = 0,6 V. $I_{SCLC} = S \times j_{SCLC}$ is the current in the SCLC region. In the high-temperature range, from the slope of the straight line and from its intercept with the current axis, according with the Eq. (6), the values E_C-E_t = 0,086 eV and N_t = 8.9×10^{15} cm^{-3} were obtained respectively.

The values of the above mentioned quantities are in good agreement with those reported before for evaporated CdS films.

$B_{1.2}$ The I - V characteristics after irradiation

The current voltage characteristics of the Au/CdS/Au cells, after irradiation with 7 MeV electrons to a fluency of 4×10^{15} e/cm^2 are shown in a linear and logarithmic plot in Fig. 5. The I - V characteristics in logarithmic plot (Fig. 5b), suggest that again two distinct conduction mechanisms are present. Following the treatment indicated

above, we obtained from $\ln(I_\Omega / U) = f(10^3 / T)$ plot (Fig. 6a), the values: E_{a2} = 0,025 eV and E_c-E_{F0} = 0,087 eV. The value of E_{a2} is a little larger than that obtained in the case of nonirradiated cells. More important, in the high-voltage range experimental results suggest rather that the plot $\ln(I / U) = f(U)$ gives a set of straight – lines. This is typical for space - charge - limited - currents in the case of a uniform traps distribution in the band - gap of the CdS layer (Fig. 6b). The uniform trap distribution may be described by:

$$\rho(E) = \frac{dN_t}{dE} \tag{7}$$

where N_t is the total density of traps distributed in the energetic band $\Delta E = E_1$-E_2, located inside the band - gap of semiconductor.

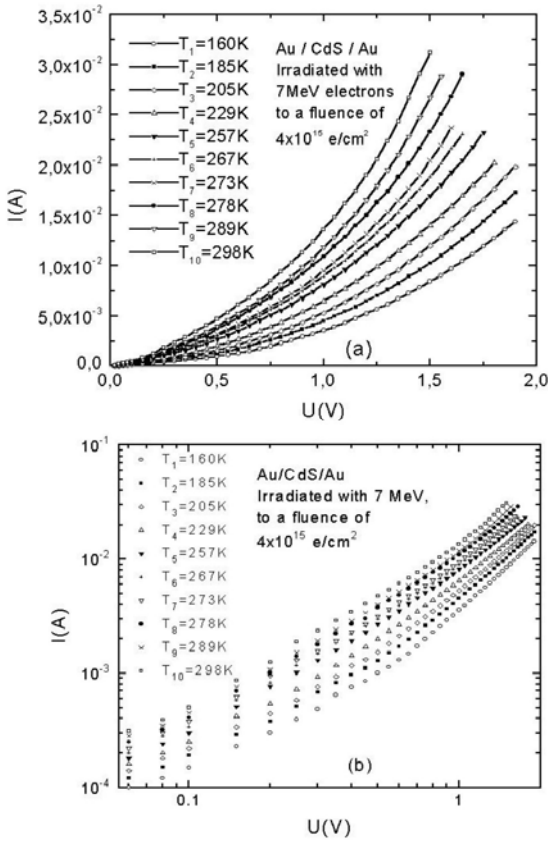

Fig. 5. The I-U characteristics for the Au/CdS/Au cells irradiated with 7 MeV electrons to a fluency of 4×10^{15} e/cm^2 , for different temperatures: (a) in linear scale; (b) in logarithmic scale.

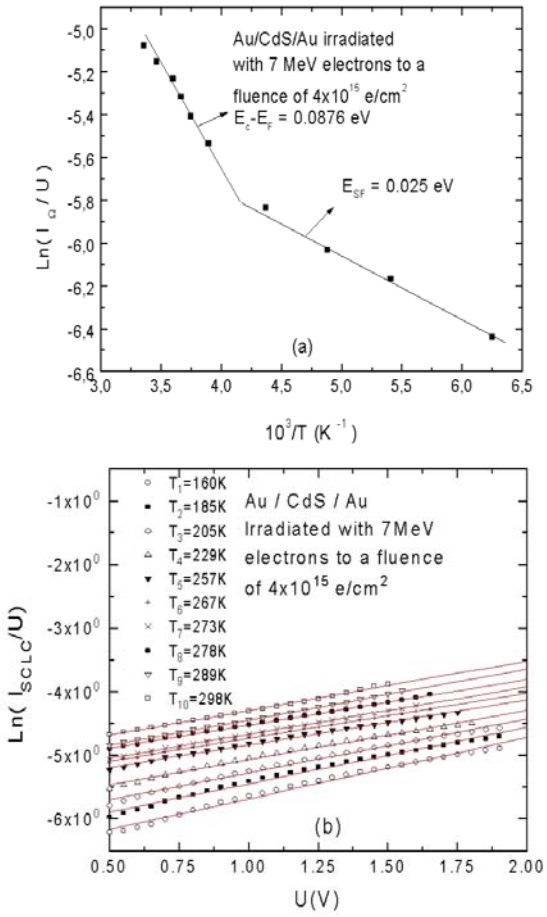

Fig. 6. The dependence of: (a) ln (I_Ω / U) = f(10^3/T) at U = 0.1 V; (b) ln (I_{SCLC} / U) = f(U), for the Au/CdS/Au cells irradiated with 7 MeV electrons to a fluency of 4×10^{15} e/cm^2.

According with Rose's treatment [20] the current density of SCLC is described by:

$$j_{SCLC} = \frac{9}{8} q\mu_0 n_0 \frac{U}{d} \exp\left(\frac{\varepsilon U}{qd^2 k_B T \rho(E)}\right) \tag{8}$$

The slope of a line (Fig. 6b) gives the value of $\rho(E)$ and its intercept on the *ln(I/U)* axis gives the possibility to find n_0 according to the equation:

$$\ln\left(\frac{I_{SCLC}}{U}\right) = \ln\left(\frac{9}{8} S \frac{q\mu_0 n_0}{d}\right) + \frac{\varepsilon}{qd^2 KT\rho(E)} U \tag{9}$$

Fitting our experimental data with eq. (9), and considering for μ_0 and N_c the above determined values, we obtained for $\rho(E)$ and n_0 the average values 6.43×10^{17} cm^{-3} eV^{-1} and 1.42×10^{16} cm^{-3}, respectively.

B2. Au/CdSe/Au sandwich cells

The current-voltage characteristics of the Au/CdSe/Au cells, before and after the two sessions of irradiation, are also nonlinear and completely symmetrical with respect to the polarity of applied voltage. The Ohm's law is followed at low applied voltage, with a thermally activated conductivity described by the eq (2), as demonstrated by the plot in Fig. 7. The values of the parameters entering eq. (2), as obtained by numerical fit, are indicated in Table 2. The values of σ_1 and E_{a1} in Table 2 correspond to the conduction band mechanism, while σ_2 and E_{a2} are typical for the hopping mechanism.

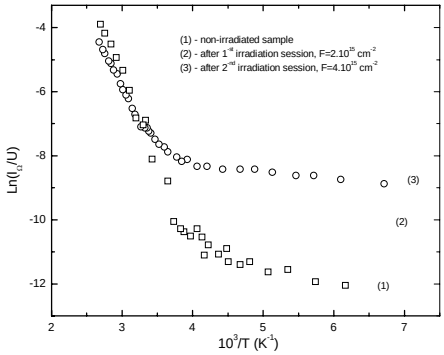

Fig. 7. Dependence of the electrical conductivity on reciprocal temperature, for the non-irradiated sample (1) and after two subsequent irradiation sessions with 7 MeV electrons to the fluencies: 2×10^{15} cm^{-2} (2) and $4\times10^{15}cm^{-2}$ (3), respectively.

Table 2. Parameters describing the electrical properties of the films and the defect band states.

	σ_1 ($\Omega^{-1}cm^{-1}$)	E_{a1}= E_c-E_{F0} (eV)	σ_2 ($\Omega^{-1}cm^{-1}$)	E_{a2} (eV)	N_0 ($cm^{-3}eV^{-1}$)	$\|E_0\|$ (eV)	ΔE (eV)
before irradiation	514.17	0.46	4.59×10^{-6}	0.048	1.09×10^{14}	0.41	0.055
after 1-st irradiation	91.44	0.42	8.54×10^{-6}	0.018	3.31×10^{14}	0.41	0.052
after 2-nd irradiation	11.47	0.37	4.69×10^{-6}	0.029	5.74×10^{14}	0.41	0.052

After irradiation a shift of the Fermi level towards CB was observed, as well as an important decrease of the pre-exponential factor σ_1. The Fermi level is pinned by some defect states of donor type, whose density is strongly affected by irradiation. Using the measured values of E_{a1} and E_{a2}, the location of these defect states in the band gap of CdSe can be determined with the following argument. The hopping activation energy E_{a2} is roughly of the order of $|E_0 - E_{F0}|$, where E_0 is the energetic separation between the center of the band of defect states and the bottom of CB E_c, and E_{F0} is the equilibrium Fermi level, also measured from E_c [21]. In the following all energetic values will be considered with respect to E_c, taken as the zero on energy scale (so E_0 , $E_{F0}<0$). If $E_0 > E_{F0}$ (the center of defect band located between the Fermi level and the bottom of CB), states lying near the Fermi level are very rare, their overlap is weak, and consequently their contribution to the hopping conductivity can be neglected. The main contribution to hopping conduction is due to electrons activated from the Fermi level into the peak of the density of states, so $E_{a2} = E_0 - E_{F0}$, or equivalently, $E_{a2} = E_{a1} - |E_0|$ (see Fig. 8). The same argument holds for the case where $E_0 < E_{F0}$ (the Fermi level located between the center of defect band and the bottom of CB), when the hopping conduction is mainly associated with the motion of the holes over defect states whose energy is close to E_0, and $E_{a2} = E_{F0} - E_0$. This seems to be the case after the second irradiation. Comparing the values of E_{a2} and E_{a1} in Table 2, a value E_0 of about -0.41 eV is obtained. The locations of the defect band and of the Fermi level before and after irradiation are indicated in Fig. 8.

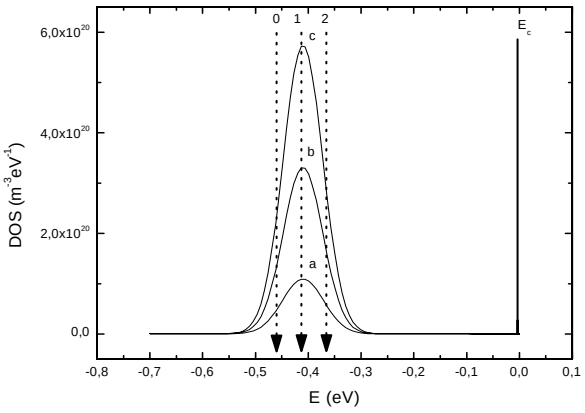

Fig. 8. Model of defect states band in the band gap of CdSe, as suggested by the analysis of the presented transport data. The irradiation influence on the location of the Fermi level (0- non-irradiated, 1-after first and 2-after the second irradiation) and also on the defect states density (a- non-irradiated, b-after first and c- after the second irradiation) are indicated.

The effect of irradiation is important also in the super-linear region of the I-V characteristics. We have interpreted the data in that range, in the frame of SCLC

theory, by considering a defect band with a Gaussian shape [13]:

$$N_t(E) = N_0 \exp\left(-\left(\frac{E-E_0}{\Delta E}\right)^2\right) \quad (10)$$

For a *n*-type material, the electric field *E(x)* in the sample is given by the Poisson equation [20]:

$$\frac{dE}{dx} = \frac{e}{\varepsilon_0 \varepsilon_r} \cdot (n - n_0 + n_t - n_{t0}), \quad E(0) = 0, \quad (11)$$

and the current density, constant through the sample, is:

$$j = e\mu_n n(x)E(x) = const. \quad (12)$$

In eq. (11) $n_0 = N_c \exp\left(\frac{E_{F0} - E_c}{k_B T}\right)$ and n_{t0} are the thermal equilibrium free and trapped carrier density, $n = N_c \exp\left(\frac{E_F - E_c}{k_B T}\right)$ and n_t denote the same quantities in the non-equilibrium case, when the carrier injection at the contacts becomes important, $\varepsilon_0 = 8.85\times10^{-12}$ F/m is the vacuum permittivity, $\varepsilon_r = 10$ is the CdSe dielectric constant, e is the electron charge, E_{F0} is the equilibrium Fermi level given in Table 2, E_F is the non-equilibrium quasi-Fermi level. Considering the effective mass of electrons in CdSe, $m_n = 0.13 \cdot m_0$, the effective density of states in the conduction band was evaluated as

$$N_c = 2\left(\frac{2\pi m_n k_B T}{h^2}\right)^{3/2} = 0.226 \cdot 10^{21} T^{3/2} \text{ m}^{-3}.$$

Assuming a set of traps distributed in energy, having the density of states $N_t(E)$, n_t can be written as:

$$n_t = \int_{E_v}^{E_c} \frac{N_t(E)dE}{1 + \frac{1}{2}\exp\left(\frac{E-E_F}{k_B T}\right)} = \int_{E_v}^{E_c} \frac{N_t(E)dE}{1 + \frac{n_0}{2n}\exp\left(\frac{E-E_{F0}}{k_B T}\right)} \quad (13)$$

The same expression holds for n_{t0}, with E_F replaced by E_{F0}. Using eqs. (10-13), the electrical field in the sample and, subsequently, the voltage across the sample, corresponding to each value of the current density can be calculated.

A numerical fit procedure was developed for determining the parameters N_0, E_0 and ΔE entering eq. (10). The center of the defect band E_0 was restricted to 0.41 eV below the bottom of the conduction band, following the argument presented above. The I-V characteristics recorded at different temperatures were used (see Fig. 9), the parameters were determined for each of them and the average results are indicated in Table 2. For the sake of simplicity only three I-V plots together with the corresponding results of the numerical fit were showed in Fig. 9.

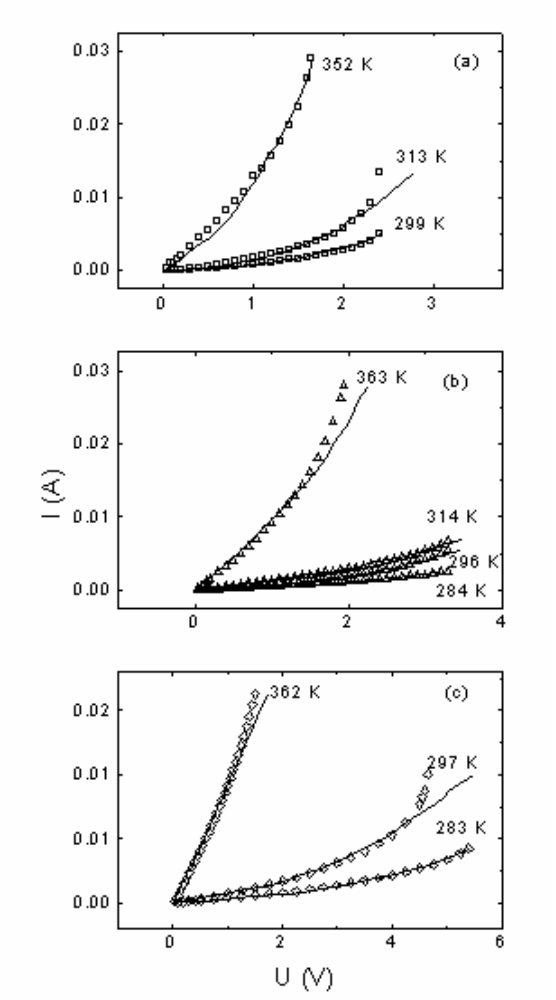

Fig. 9. Current-voltage characteristics at different temperatures: before (a), after the first (b) and second (c) irradiation sessions, respectively. Both the measured values (points) and the best fits (continuous line) obtained as indicated in text are plotted.

For comparing purposes the characteristics recorded at about the same temperatures, for non-irradiated and irradiated structures, have been chosen.

As expected, an increase of the defect state density from 1.09×10^{14} cm^{-3}eV^{-1} for the non-irradiated sample to 5.74×10^{14} cm^{-3}eV^{-1} after the second session of irradiation was observed. There is no significant change of the width ΔE=0.11 eV of the defect band.

B3. Planar CdSe structures

B3.1 Temperature dependence of the electrical resistance

The Arrhenius plot of the measured electrical resistance is shown in Fig. 10. One can easily observe that electron irradiation (6 MeV electrons to a fluency of 5×10^{13} electrons/cm^2) induced only slight changes in

electrical properties, except for temperatures below 90 K. In some temperature ranges, the temperature dependence of the films resistance is well described by:

$$R(T) = R_0(T)\exp\left(\frac{E_a}{k_B T}\right) \quad (14)$$

where E_a is the activation energy. The pre-exponential factor R_0 may have a slight temperature dependence, reflecting, for example, the temperature dependence of free carriers mobility in the case of band conduction mechanism. Table 3 presents the values of E_a and R_0 parameters appearing in eq. (14), as obtained by numerical fit in the indicated temperature ranges. A band conduction mechanism is responsible for the observed electrical properties at room temperature and down to 240 K, controlled essentially by a deep donor level located at 0.37 eV below the bottom edge of the conduction band. In this region the temperature dependence of the electrical resistance is entirely due to the rapid decrease in the concentration of the free carriers (electrons), gradually recaptured by the donor levels they originate from. An increase of the pre-exponential parameter, R_0, was observed after irradiation, which can be explained by the increase of the density of defect states in the films, and the corresponding decrease of the mobility of the free carriers.

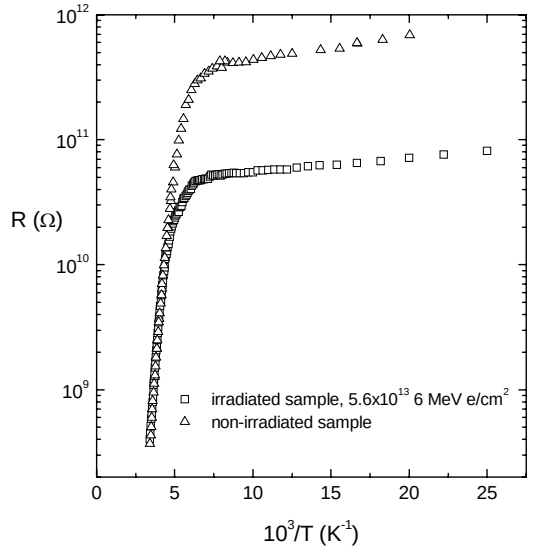

Fig. 10. Temperature dependence of the electrical resistance of the CdSe films, before and after irradiation with 6 MeV, 5×10^{13} electrons/cm^2.

One can easily observe more significant changes after irradiation in the low temperature range, below 90 K (Fig. 10). E_a and R_0 values in this range, as well as the effect of irradiation, can be explained assuming that the electrical conduction comes from electrons hopping between the main donor states, partially emptied by compensation. Unlike the room temperature case, the pre-exponential factor R_0 drops by almost an order of magnitude after irradiation. This is typical for hopping conduction mechanism, when R_0 depends exponentially on the density of localized states involved in the process [21].

C. Proton irradiated samples

C1 Electrical properties

Figs. 11 and 12 show the electrical resistance of two films (CdS and CdSe, respectively), in logarithmic scale versus the reciprocal of temperature. Proton irradiation in the above-indicated conditions induced only slight changes in electrical properties, except for temperatures below 100 K. The resistance is thermally activated, its temperature dependence being well described by eq. (14).

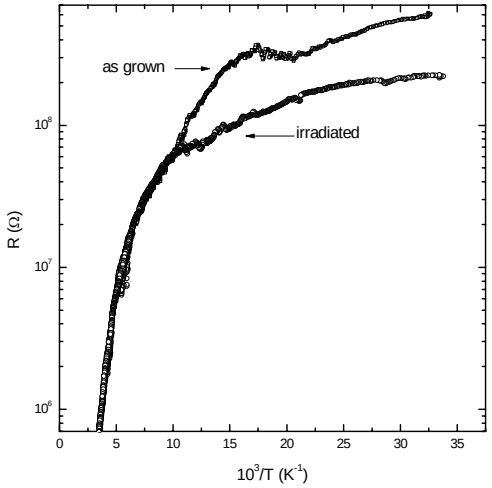

Fig. 11. Temperature dependence of the electrical resistance of the CdS films, before and after irradiation with 3 MeV, 3×10^{13} protons/cm^2.

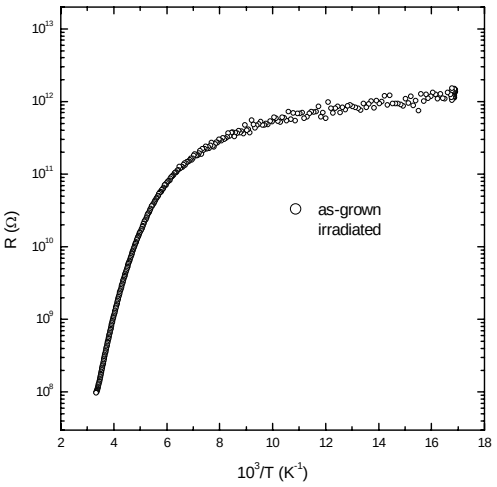

Fig. 12. Temperature dependence of the electrical resistance of the CdSe films, before and after irradiation with 3 MeV, 3×10^{13} protons/cm^2.

E_a and R_0 parameters, as obtained by numerical fit in the indicated temperature ranges are collected in Table 3. In both cases, at room temperature and down to 240 K, the experimental results suggest a band conduction mechanism, controlled essentially by donor levels located at 0.34 eV (CdSe) and 0.174 eV (CdS) below the bottom edge of the conduction band. After irradiation the activation energy shifts to 0.40 eV in the case of CdSe film and to 0.196 eV in the case of CdS. Note also the constant activation energies (E_{a1}=0.113 eV, E_{a2}=0.029 eV for as-grown sample and E_{a1}=0.065, E_{a2}=0.027 eV after irradiation, respectively) existing in rather limited temperature ranges in the case of CdS sample. This can be explained as due to the hopping of the charge carriers, thermally excited from the main donor, over some compensated donor states, located in energy at E_{a1} and E_{a2} above the main donor. The number of hopping electrons is exponentially small $\left(\propto e^{-\frac{E_{a1,2}}{k_B T}} \right)$, but their mobility is larger, due to a larger localization radius of the states with levels closer to conduction band. For that reason the above-mentioned mechanism could become dominant in a finite temperature range.

More important changes occur after irradiation in the low temperature range, below 90 K (Fig. 11 and Fig. 12). E_a and R_0 values in this range can be explained assuming that the electrical conduction comes from electrons hopping over main donor states, partially emptied by compensation.

C2 Thermally stimulated currents

TSC spectra analysis, performed both before and after irradiation, allowed us to obtain a more detailed quantitative information on the effect of proton irradiation on the CdSe and CdS films. A well resolved TSC peak, originating from thermal release of charge carriers from a trap having activation energy E_{t0} into conduction or valence band, is described by [22]:

$$I_{TSC}(T) = I_0 \exp\left(-\int_{T_0}^{T} \frac{e_t}{\beta} dT' \right), \qquad (15)$$

where $I_0 = Ce\mu\tau N_t e_t V$, e is the electron charge, μ and τ are, respectively, the mobility and lifetime of free carriers, V is the applied voltage, C is a geometrical factor, N_t is the trap density, T_0 is the starting temperature, β is the heating rate and e_t is the emission rate from the trap, given by:

$$e_t = \frac{16\pi m^* k_B^2}{h^3} \sigma_t T^2 \exp\left(-\frac{E_{t0}}{k_B T} \right). \qquad (16)$$

In eq. (16) m^* is the free carrier effective mass, h is Planck's constant, k_B is Boltzmann's constant, σ_t is the free carrier capture cross-section and E_{t0} is the ionization energy of the traps. Usually, the temperature dependence of σ_t can be expressed as $\sigma_t = \sigma_{t0} \exp\left(-E_\sigma / k_B T \right)$ and the experimentally measured trap activation energy is then $E_t = E_{t0} + E_\sigma$.

Figs. 13 and 14 show the normalized TSC spectra measured before and after proton irradiation, in the case of CdSe and CdS films, respectively. We have used the normalization procedure, introduced previously by Look et al., [23,24]. This procedure is based on the observation that both TSC and photocurrent I_{PC} are proportional to lifetime τ and mobility μ of the carriers, and therefore, their ratio I_{TSC}/I_{PC} should only depend on quantities that can be obtained by fit. In this way complete quantitative results can be extracted from TSC data. In case of thin films (αd<<1, α being light absorption coefficient and d the film thickness), the photocurrent is given by $I_{PC} = Ce\mu\tau\Phi_0\alpha V$, where Φ_0 is the incident light flux and C the geometrical factor entering eq. (15). The I_{TSC}/I_{PC} ratio is then given by:

$$\frac{I_{TSC}}{I_{PC}} = \frac{N_t e_t \exp\left(-\int_{T_0}^{T} \frac{e_t}{\beta} dT' \right)}{\Phi_0 \alpha}. \qquad (17)$$

Both spectra consist of several heavily overlapped peaks and a direct use of eq. (17) for any of them is not adequate. To reduce the interference of neighboring peaks, a fractional heating technique was used: after illumination the sample was heated with constant rate to a temperature 2-3 K larger than that corresponding to a maximum or shoulder in TSC spectrum, it was maintained at that value for 5 min., then the sample was cooled down to a temperature 30 K lower and the cycle was repeated. It is expected that by such a procedure shallower levels are gradually emptied and their influence on the deeper ones reduced. However, some peaks are to close to each other to be experimentally resolved, even by fractional heating, and a simultaneous fit with two features described by eq. (18) had to be performed, especially for the low temperature region.

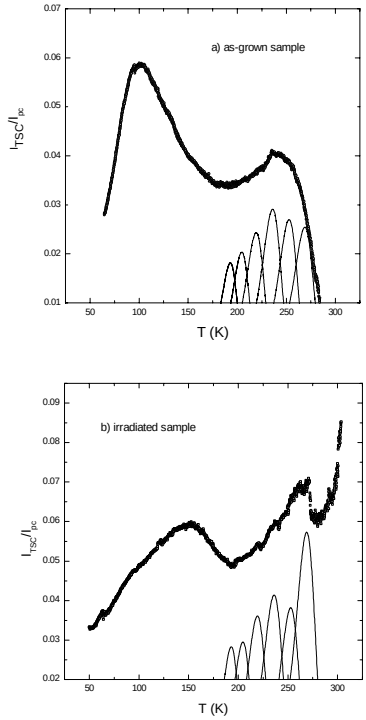

Fig. 13. Normalized TSC spectra of CdSe sample, recorded before (a) and after (b) irradiation with 3 MeV, 3×10^{13} protons/cm^2. The contribution of individual peaks most affected by irradiation, extracted as explained in text, is shown.

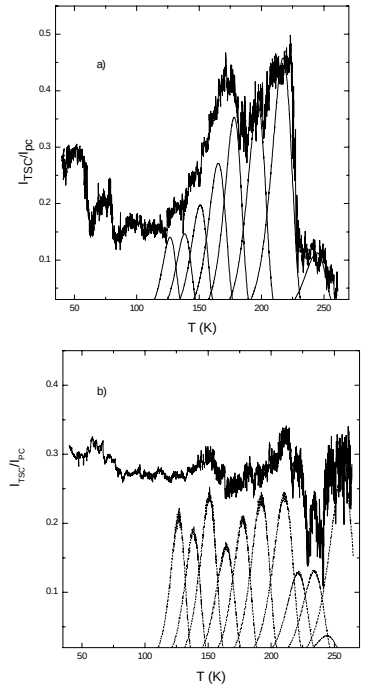

Fig. 14. Normalized TSC spectra of CdS sample, recorded before (a) and after (b) irradiation with 3 MeV, 3×10^{13} protons/cm^2. The contribution of individual peaks most affected by irradiation, extracted as xplained in text, is shown.

Table 3. Parameters characterizing the electrical resistance (eq. (14)), as obtained by numerical fit.

Temperature range (K)	E_{ac} (eV)	R_0 (Ω)	Notes
240 - 300	0.37	165.5	
40 - 100	0.004	2.84×10^{11}	CdSe sample, as grown
240 - 300	0.37	248.8	CdSe sample,
40 - 100	0.003	3.87×10^{10}	irradiated (6 MeV electrons, 5×10^{13} electrons/cm^2
220 - 300	0.174	499.9	
190 - 215	0.113	1.041×10^{4}	CdS sample, as
80 - 120	0.029	2.241×10^{6}	grown
< 40	5.6×10^{-3}	8.293×10^{7}	
240 K - 300	0.196	236.4	
185 - 210	0.065	1.485×10^{5}	CdS sample,
110 - 145	0.028	2.643×10^{6}	irradiated (3 MeV
< 50	3.4×10^{-3}	7.187×10^{7}	protons, 3×10^{13} protons/cm^2)
240 - 300	0.341	160.8	
< 90	8.6×10^{-3}	2.31×10^{11}	CdSe sample, as grown
250 - 300	0.401	29.8	CdSe sample,
< 90	6.0×10^{-3}	1.05×10^{12}	irradiated (3 MeV protons, 3×10^{13} protons/cm^2)

The values of the parameters E_t, σ_{t0}, and N_t obtained at this stage were then used as initial guess for a simultaneous fit of the spectra with sums of features given by eq. (18). After this step E_t and σ_{t0} values remained practically unchanged, while pre-exponential factors N_t were modified. This was to be expected, since the repeated heating-cooling cycle modifies the initial concentrations of trapped electrons for peaks corresponding to deeper levels overlapping with analyzed ones. The trap parameters, as obtained by this procedure, are indicated in Tables 4 and 5. The most important effect of proton irradiation can be seen in the high temperature region of the spectra. In addition to the increase of the densities of some traps, new centers were identified after irradiation respectively T^*_1 şi T^*_2 traps in CdS and T^*_1 trap in CdSe.

Table 4. Parameters characterizing the traps most affected by proton irradiation (3 MeV protons, 3×10^{13} protons/cm^2), for CdSe sample. The traps are indexed following their position in the spectra, from right to left.

Trap	E_a **(eV)**	N_t **(cm^{-3})** [a]	N_t **(cm^{-3})** [b]	σ_{t0} **(cm^2)**
T^*_1	0.71	-	-	-
T_2	0.61	1.60×10^{15}	3.27×10^{15}	7.0×10^{-17}
T_3	0.556	1.67×10^{15}	4.34×10^{15}	3.6×10^{-17}
T_4	0.47	1.84×10^{15}	2.62×10^{15}	3.1×10^{-18}
T_5	0.42	1.46×10^{15}	2.18×10^{15}	1.8×10^{-18}
T_6	0.401	1.11×10^{15}	1.62×10^{15}	5.1×10^{-18}
T_7	0.38	1.06×10^{15}	1.47×10^{15}	5.1×10^{-18}

[a] as grown sample; [b] irradiated sample

Table 5. Parameters characterizing the traps most affected by proton irradiation (3 MeV protons, 3×10^{13} protons/cm^2), for CdS sample. The traps are indexed following their position in the spectra, from right to left.

Trap	E_a (eV)	N_t (cm^{-3}) [a]	N_t (cm^{-3}) [b]	σ_{t0} (cm^2)
T_1*	0.581	-	4.38×10^{16}	5.1×10^{-17}
T_1	0.545	1.73×10^{15}	5.70×10^{14}	1.4×10^{-14}
T_2*	0.531	-	1.89×10^{16}	7.1×10^{-17}
T_2	0.48	5.99×10^{16}	1.83×10^{16}	2.5×10^{-17}
T_3	0.443	3.30×10^{16}	3.34×10^{16}	1.4×10^{-17}
T_4	0.41	3.44×10^{16}	2.97×10^{16}	2.5×10^{-17}
T_5	0.368	3.90×10^{16}	2.43×10^{16}	1.8×10^{-17}
T_6	0.298	3.34×10^{16}	2.06×10^{16}	8.6×10^{-19}
T_7	0.271	2.26×10^{16}	2.72×10^{16}	9.1×10^{-19}
T_8	0.243	1.57×10^{16}	1.99×10^{16}	7.3×10^{-19}

C3 Optical properties

Fig. 15 shows the optical absorption spectra recorded in the case of a CdS film before and after irradiation. As expected for such a small fluency, there are no significant changes, except for a small red-shift of the optical threshold. The direct band gap, as estimated from:

$$A = const. \cdot \frac{(h\nu - E_g)^{1/2}}{h\nu} \quad (18)$$

shifted from 2.27 eV before irradiation to 2.24 eV after irradiation with 3 MeV protons, 3×10^{13} protons/cm^2 (Fig. 16). More important changes were observed in the photoluminescence (PL) spectra, recorded at room temperature (298 K) using 514 nm light for optical excitation (Fig. 17). After proton irradiation an increase of the broad feature centered at 751 nm (1.65 eV) was observed. That feature seems to consist of three heavily overlapped PL peaks at 733.8 nm, 756.4 and 780.4 nm respectively, associated to free-to-bound transitions. The energies corresponding to those transitions are close to ionization energy of an electron trap associated to a V_S-V_S complex [25-26]. Their presence in the spectrum recorded before irradiation, and the PL intensity increase after proton irradiation support that assignment.

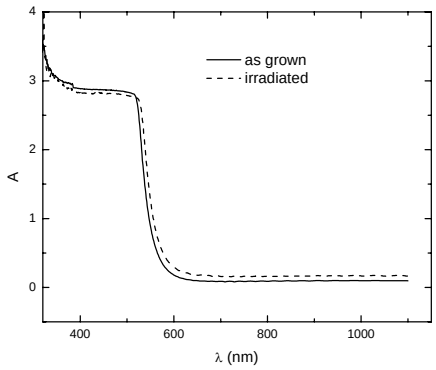

Fig. 15. Optical absorption spectra of CdS sample before and after irradiation with 3 MeV, 3×10^{13} protons/cm^2.

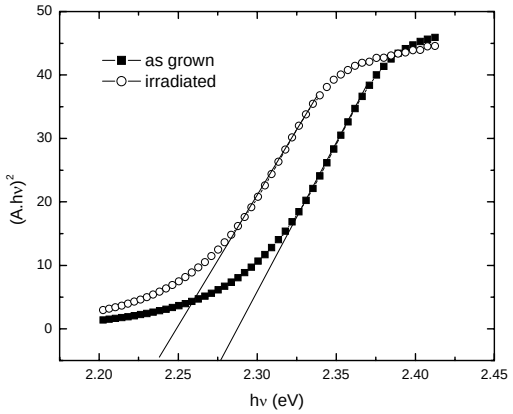

Fig. 16. Optical absorption spectra near band gap for a CdS film, before and after irradiation with 3 MeV, 3×10^{13} protons/cm^2.

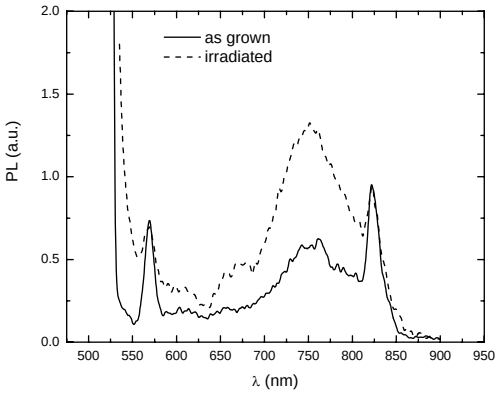

Fig. 17. Photoluminescence of a CdS film before and after irradiation with 3 MeV, 3×10^{13} protons/cm^2.

4. Discussion

The experimental results clearly demonstrated that electrical behavior of CdS and CdS thin films is induced by some defect centers, whose density is significantly increased by irradiation with electrons or protons having energies in MeV range.

It is difficult to establish the origin of defects identified by the above-indicated experimental procedures. This task is further complicated in the case of thin films, where local structural disorder exists at grain boundaries or surface and can lead to a broadening of otherwise well defined levels. However, the simplest defects presumably to act as deep donors in CdS or CdSe are chalcogen vacancies. Such defects are also very likely to be produced by electron irradiation. The peculiarity of irradiation with high-energy (in MeV range) electrons consists in the fact that it produces a few atomic displacements. The maximum energy transferred at impact by an electron having an energy E to an atom of mass M is given by [27]:

$$E_m = 2\frac{m_0}{M}E\left(2+\frac{E}{m_0c^2}\right). \quad (19)$$

For an initially 6 MeV electron, the maximum energy transferred to a Cd atom is 802 eV, to a S atom is 2815 eV, while for a Se atom it is 1140 eV. The threshold energy for atomic displacement in CdS is 7.3 eV for Cd atom and 8.7 eV for S atom [7,28]. To our knowledge, those values are unknown for CdSe and a displacement energy of 10 eV will be assumed, given that experimentally determined threshold energy for semiconductors ranges from about 6 eV to 12 eV (Ref. 27, p. 229). Then each primarily knock-on atom can produce up to 50 secondary displacements. The rate of energy loss of incident electrons is of the order of 10 MeV/cm [18] and consequently the electron energy loss in our samples is negligible, which implies that the irradiation generated Frenkel (interstitial-vacancy) pairs are uniformly distributed in volume. Some of them disappear by direct recombination. But it is plausible that interstitials, having larger mobility than vacancies, will more easily migrate among vacancies, eventually being trapped by other defects at surface or grain boundaries. Consequently, some of the vacancies produced by electron irradiation will survive the recombination process. They could also form aggregates and/or interact with oxygen atoms residually present in the vacuum chamber. The traps with increasing density after irradiation could be this type of defects.

The same defects are also likely to be produced by proton irradiation. Primary defects produced by incident protons are Frenkel pairs. The maximum energy transferred at impact by a proton having an energy E to an atom of mass M is given by [27]:

$$E_m = 4\frac{m_p}{M}E. \quad (20)$$

For an initially 3 MeV proton, the maximum energy transferred to a Cd atom is 107 keV, while for a Se atom it is 152 keV (375 keV for the S atom). Using a hard-sphere collision model, it results that each primarily knock-on atom can produce an average number of $\tilde{n} = E_i / 4E_{td} \approx 1.5\times10^4$ secondary displacements. Consequently, proton irradiation will cause a more significant structural damage as compared with electrons.

In addition, the introduction of protons can lead to passivation of dangling bonds and, as a consequence, to the conversion of some defects to trap centers of a different nature. That seems to be the case for T^*_1 şi T^*_2 traps in CdS and T^*_1 trap in CdSe (see Tables 4 and 5).

5. Conclusions

We presented in this paper an investigation by various techniques on the effects of electron and proton (energies in MeV range) irradiation on electrical properties of CdS and CdSe thin films grown by vacuum thermal deposition.

XRD spectra revealed that the films consist of hcp wurtzite phase, preferentially oriented with (001) crystalline direction perpendicular to their surface. Within the limits of experimental resolution, no change in diffraction pattern aspect or in line broadening was observed following electron irradiation at fluencies up to 10^{17} electrons/cm^2. It follows then that irradiation with 6 or 7-MeV electrons results in the creation of point-like defects.

Electrical properties of the films were investigated using two different geometries, Au/(CdS, CdSe)/Au sandwich cells and planar structures with four Al contacts deposited on top of the films, respectively. In the case of Au/CdS/Au structures, I-V characteristics recorded at different temperatures, interpreted in the frame of SCLC theory, revealed that electrical behavior of as-grown films is controlled by a single trap, while after irradiation a distribution of traps is responsible for the recorded I-V dependence. In the case of Au/CdSe/Au structures, a model was developed in the frame of SCLC theory [13] with a more realistic energetic distribution of traps, to account for the observed I-V dependence. The results are in good agreement with those obtained from TSC curves measured in the case o planar structures.

In CdSe films, an extrinsic conduction determined by the presence of a main donor center located at 0.34-0.40 eV below the conduction band bottom edge was observed in the high temperature range (room temperature and below, to 240 K). At low temperatures charge transport occurs through hopping mechanism; in that temperature range the effect of irradiation is more pronounced. The density of localized states involved in the hopping process is increased by irradiation, consequently the overlap of their corresponding wave functions increases, which results in exponentially smaller resistance values.

From TSC spectra analysis, several traps were identified in the band gap. The above mentioned deep donors with ionization energy of 0.34-0.40 eV, which mainly controls electrical behavior of the films, exists in larger densities. The TSC procedure we used allows for an accurate determination of trap parameters (see Tables 4 and 5).

PL spectra recorded for CdS samples consist of several well defined peaks and some broad features. After proton irradiation a significant increase of the intensity of the PL feature located at 751 nm occurred. We believe that that feature is related to a S-divacancy defect. The origin of the other identified defects, with smaller ionization energies, remains unknown at this time.

References

[1] G. Jäniche, H. Berger, J. Vac. Sci. Tech., **6**, 552 (1969).
[2] H. Berger, G. Jäniche, N. Grachovskaya, phys. status solidi, **33**, 417 (1969).
[3] R. Bube, L. Barton, J. Chem. Phys., **29**, 128 (1958).
[4] K. Shimizu, Japan. J. Appl. Phys., **4**, 627 (1965).
[5] S. Antohe, L. Ion, V. A. Antohe, Romanian Journal of Physics, **48**, 511 (2003).
[6] R. D. Gould, B. B. Ismail, Int. J. Electron. **69**, 19-24 (1990).

[7] B. A. Kulp, Phys. Rev. **125**, 1865 (1962).
[8] H. Ohyama, K. Hayama, phys. status solidi (a) **142**, K.117 (1994).
[9] I. Spânulescu, I. Secareanu, N. Bâltâteanu, I. Z. Abdi, T. Khalass, Thin Solid Films **143**, 1 (1986).
[10] V. Ruxandra, S. Antohe, J. Appl. Phys. **84**, 727 (1998).
[11] J. Dresner, F. V. Shallcross, Solid-State Electronics, **5**, 205 (1962).
[12] J. Dresner, F. V. Shallcross, J. Appl. Phys. **34**, 2391 (1963).
[13] S. Antohe, L. Ion, V. Ruxandra, J. Appl. Phys. **90**, 5928 (2001).
[14] S. Antohe**,** L. Ion, V. A. Antohe, J. Optoeletron. Adv. Mater. **5** (4) 801-816 (2003).
[15] L. Ion, S. Antohe, M. Popescu, F. Scarlat, F. Sava, Felicia Ionescu, J. Optoelectron. Adv. Mater. **6**(1), 113-119 (2004).
[16] V. Ruxandra, J. Mater. Sci. Lett. **16**, 1833 (1997).
[17] P. Cristea, I. Spânulescu, I. Secâreanu, V. Ruxandra, S. Spânulescu, N. Baltâteanu, J. Mat. Sci. Lett. **12**, 1467 (1993).
[18] J. W. Corbett, "Electron Radiation Damage in Semiconductors and Metals" (Solid State Physics Series, Vol. 7(suppl.), Academic, New York, 1966).
[19] E. F. Kaelble (ed.), "Handbook of X-Rays", McGraw-Hill, New York, USA, 1967, chapt. 17.
[20] M. A. Lampert, P. Mark, "Current Injection in Solids" (Academic Press, New York, 1970), pp. 33-38.
[21] B. I. Shklovskii, A. L. Efros, "Electronic Properties of Doped Semiconductors" (Springer, Berlin, 1984), chapt. 6.
[22] D. C. Look, in Semiconductors and Semimetals, edited by R. K. Willardson and A. C. Beer, (Academic, New York, 1983), Vol. 19, p. 75.
[23] D. C. Look et al., Phys. Rev. **B55**, 2214 (1997).
[24] Z-Q. Fang, D. C. Look, Appl. Phys. Lett. **59**, 48 (1991).
[25] J. Oualid, D. Surts, J. Gervais, S. Martinuzzi, J. Phys. C: Solid State Phys., **12**, 2313 (1979).
[26] J. P. Sorbier, J. Oualid, S. Martinuzzi, J. Phys. C: Solid State Phys., **12**, 2323 (1979).
[27] J. Bourgoin, M. Lannoo, "Point Defects in Semiconductors" II (Solid State Sciences Series, Vol. 35, Springer, Berlin, 1983), chapt. 8.
[28] B. A. Kulp, R. H. Kelley, J. Appl. Phys., **31,** 1057 (1960).
[29] L. Ion, S. Antohe, J. Appl. Phys., Vol. **97** (1), January 1, 3513-3516 (2005).

*Corrsponding author: santohe@solid.fizica.unibuc.ro